AGU PUBLICATIONS

JGR

Journal of Geophysical Research: Atmospheres

RESEARCH ARTICLE
10.1002/2016JD025312

The properties of optical lightning flashes and the clouds they illuminate

Michael Peterson[1], **Wiebke Deierling**[2], **Chuntao Liu**[3], **Douglas Mach**[4], **and Christina Kalb**[1]

[1]National Center for Atmospheric Research, Boulder, Colorado, USA, [2]Department of Aerospace Engineering, University of Colorado Boulder, Boulder, Colorado, USA, [3]Department of Physical & Environmental Sciences, Texas A&M University, Corpus Christi, Texas, USA, [4]USRA, Huntsville, Alabama, USA

Key Points:
- Optical lightning measurements can be used to identify propagating flashes
- Flash characteristics are sensitive to cloud properties that affect scattering
- Oceanic flashes are still larger and more energetic when they occur in similar cloud regions as their land-based counterparts

Correspondence to:
M. Peterson,
michaeljp24@gmail.com

Citation:
Peterson, M., W. Deierling, C. Liu, D. Mach, and C. Kalb (2017), The properties of optical lightning flashes and the clouds they illuminate, *J. Geophys. Res. Atmos.*, *122*, 423–442, doi:10.1002/2016JD025312.

Received 2 MAY 2016
Accepted 26 OCT 2016
Accepted article online 31 OCT 2016
Published online 13 JAN 2017

Abstract Optical lightning sensors like the Optical Transient Detector and Lightning Imaging Sensor (LIS) measure total lightning across large swaths of the globe with high detection efficiency. With two upcoming missions that employ these sensors—LIS on the International Space Station and the Geostationary Lightning Mapper on the GOES-R satellite—there has been increased interest in what these measurements can reveal about lightning and thunderstorms in addition to total flash activity. Optical lightning imagers are capable of observing the characteristics of individual flashes that include their sizes, durations, and radiative energies. However, it is important to exercise caution when interpreting trends in optical flash measurements because they can be affected by the scene. This study uses coincident measurements from the Tropical Rainfall Measuring Mission (TRMM) satellite to examine the properties of LIS flashes and the surrounding cloud regions they illuminate. These combined measurements are used to assess to what extent optical flash characteristics can be used to make inferences about flash structure and energetics. Clouds illuminated by lightning over land and ocean regions that are otherwise similar based on TRMM measurements are identified. Even when LIS flashes occur in similar clouds and background radiances, oceanic flashes are still shown to be larger, brighter, longer lasting, more prone to horizontal propagation, and to contain more groups than their land-based counterparts. This suggests that the optical trends noted in literature are not entirely the result of radiative transfer effects but rather stem from physical differences in the flashes.

1. Introduction

Lightning measurements are an important resource because they can be used for combination of practical applications for safeguarding lives and livelihoods (i.e., Lightning Jump Algorithms [*Schultz et al.*, 2009]) and research applications for diagnosing convective intensity [i.e., *Cecil et al.*, 2005] and making inferences about convective processes within thunderstorms [i.e., *Deierling and Petersen*, 2008]. The Tropical Rainfall Measuring Mission (TRMM) has been a particularly powerful tool for probing the structure of thunderstorms and building relationships with total lightning activity. Its unique sensor payload included a precipitation radar (PR), TRMM Microwave Imager (TMI), Visible and Infrared Scanner (VIRS), and Lightning Imaging Sensor (LIS) [*Kummerow et al.*, 1998]. It was in orbit between December 1997 and mid-2015, providing an unparalleled record of lightning measurements from low Earth orbit alongside observations from the other TRMM sensors over a global domain that included the tropics and subtropics up to 36° latitude.

The large spatial and temporal domains of TRMM make it possible to assess the variability of thunderstorms across large spatial and temporal scales. The Algorithm Theoretical Basis Document for LIS that was created as part of the mission planning process [*Christian et al.*, 2000] recognizes climate monitoring applications as a core justification for lightning measurements on TRMM. As electrification is closely related to the convective updraft, large-scale changes in convection that result from climate variability (for example, El Niño–Southern Oscillation) should be manifested in the global electricity measurements provided by instruments like LIS. Lightning flash rates and surface-based electric fields are used as diagnostics of the Global Electric Circuit (GEC [*Williams*, 2009]), a series of electrical connections that describe the large-scale flow of electricity within the atmosphere and serve to maintain the electrical potential of the ionosphere relative to the Earth's surface. Within this circuit, charge imbalances in electrified clouds—thunderstorms and electrified shower clouds (ESCs)—produce conduction (Wilson) currents that interact directly with the ionosphere. Aircraft measurements indicate that the majority of electrified clouds (93% [*Mach et al.*, 2009]) produce upward directed Wilson currents that contribute to the GEC while the remaining produce downward currents that would "short" the circuit.

As the entire atmosphere falls on the same circuit, it is reasonable to expect that the source current (global electrified weather) would correlate well with the return current (fair-weather electric fields). However, the diurnal variation of LIS total lightning differs from the diurnal variation of surface-based fair weather electric field measurements in Antarctica [*Burns et al*., 2005] and the Carnegie curve [*Whipple*, 1929]. The diurnal cycle of total lightning has an amplitude that is greater than the Carnegie curve and places an unmatched emphasis on Africa over the Americas and Asia. These discrepancies are largely attributed to the effect of ESCs that would be omitted in the LIS/Optical Transient Detector climatology described in *Cecil et al*. [2014]. *Mach et al*. [2011] used observations from the NASA ER-2 aircraft to adjust the climatology to account for these clouds, but questions remain concerning lightning and Wilson currents, and implications for the GEC. These questions are particularly important for modeling efforts that aim to describe the electrical system of the Earth from the surface to the ionosphere [*Hays and Roble*, 1979; *Lucas et al*., 2015].

At the forefront of these questions is the issue of the observed differences between land-based and oceanic thunderstorms. It is well documented that most lightning occurs over land [*Landsberg*, 1960; *Court and Griffiths*, 1982; *Orville and Henderson*, 1986; *Christian et al*., 2003; *Williams et al*., 2004; *Lay et al*., 2007; *Liu et al*., 2010; *Mach et al*., 2010; *Mach et al*., 2011] despite the fact that the oceans account for 71% of the Earth's surface area. This is largely due to the relative frequency of occurrence (or cell spacing) of intense thunderstorms [*Boccippio et al*., 2000] as well as differences in their size and maturity spectra [*Bang and Zipser*, 2015]. However, ER-2 overflights of thunderstorms and shower clouds show that Wilson currents from oceanic storms are twice as strong, on average, as their land-based counterparts while lightning was only observed in 43% of oceanic overflights compared to 78% of overflights over land [*Mach et al*., 2010]. That typical oceanic storms can simultaneously produce less lightning, and stronger conduction currents suggest that there may be a fundamental difference between land and ocean electrified weather that is important for understanding the GEC.

Another perspective on land and ocean storm differences comes from the measured properties of lightning flashes. Measurements by ground-based lightning networks suggest that oceanic storms are associated with higher peak current discharges compared to their onshore counterparts [*Orville and Huffines*, 2001; *Hutchins et al*., 2013]. If discharges are stronger over the ocean, it might help to reconcile how oceanic storms can produce stronger electric fields compared to land and yet less lightning. However, these results may be hindered by systematic limitations of the ground-based sensors. The increased conductivity of seawater that might minimize signal attenuation has been considered and ruled out due to a lack of an observed abrupt change at the coastline with positive polarity flashes [*Orville and Huffines*, 2001], but the possibility of other biases resulting in the observed high currents remains. For example, the spatial variability in lightning sensor density may impact the lightning localization and peak current calculations.

Similar trends can be noted in the measured characteristics of optical flashes, where oceanic flashes appear to be larger and brighter than those over land. Unlike the ground-based sensors, instruments such as LIS sample land and ocean regions at the same detection efficiency regardless of the distance from shore. However, optical observations have their own set of caveats and limitations. Chief among them is the issue that optical measurements are the end result of a complex radiative transfer problem that involves optical emission along the lightning channel, scattering within the cloud, and the detection of optical signals by the sensor. Any of these factors may influence whether a flash is detected and what its measured properties will be. A simple example is the background radiance that varies by solar angle. When the Sun is directly overhead, it becomes more difficult for LIS to distinguish optical lightning transients from the high background radiance. This results in a detection efficiency that varies from ~69% at noon to ~88% at night [*Cecil et al*., 2014]. Because of these radiative transfer concerns, *Boccippio et al*. [2000] concluded: "we are as yet unable to determine whether [ocean flashes appearing brighter and larger] is due to differences in the energetics of the flashes or the optical scattering properties of storm cells or some combination of the two."

The purpose of this study is to explore the optical characteristics of LIS flashes and the properties of the surrounding cloud regions in order to address some of these radiative transfer concerns. These issues are particularly important due to a recent interest in subflash level LIS observations [i.e., *Koshak*, 2010; *Peterson and Liu*, 2013] that may be able to provide information on flash structure, as well as the increased availability of optical lightning measurements following the launch of the GOES-R satellite that will include a Geostationary Lightning Mapper (GLM [*Goodman et al*., 2013]) and the deployment of LIS on the International Space Station (ISS-LIS [*Blakeslee et al*., 2014]). A focus will be placed on investigating land

and ocean differences in flash energetics. This will be addressed by identifying LIS flashes that illuminate otherwise similar cloud regions in land and ocean storms. Finally, new applications of event- and group-level optical flash data are proposed including the identification of flashes that propagate with time and may be examples of horizontal breakdown structures (for example, spider lightning).

2. Data and Methodology

2.1. An Illuminated Cloud Feature Database

The central piece of this study is the creation of a TRMM cloud feature database that describes the radar, passive microwave, and infrared properties of the storm regions where LIS flashes are observed. Previous studies examining the properties of thunderstorms and lightning activity have used radar precipitation features (RPFs [*Liu et al*., 2008]) to distinguish between thunderstorm regions of interest. RPFs are defined as contiguous raining areas based on TRMM PR reflectivity data. They are typically storm-scale features, but often reach the mesoscale in certain regions and storm types. While this approach is suitable for assessing the overall properties of thunderstorms such as flash rates, these features are significantly larger than the typical spatial scales of lightning discharges. Particularly in the case of mesoscale convective systems (MCSs) and tropical cyclones, the properties of the system as a whole may be entirely different than those of the local cell that produces a flash or the specific storm region that the flash is embedded in. Examples would include cases of multicell storms or convective systems that have large areas of stratiform and anvil cloud [*Peterson and Liu*, 2011]. As a first approach, *Peterson and Liu* [2013] examined the properties of the storm at the precise location of the lightning flash centroid. However, even in the case of typically small features like lightning flashes, a single PR or TMI pixel may not always be representative of the entire storm region of interest. Some flashes, for example, illuminate a large area while even the majority of small flashes occur in convective storm regions where gradients in storm properties are common. For this reason, a more integrative approach is required to describe the properties of the storm region that the radiance produced by the flash would have to traverse to reach LIS.

The approach employed by this study is to create a new type of cloud feature from event pixel-level LIS data. These features bound regions of the parent storm that are illuminated by each LIS flash and are a departure from the TRMM features in literature that rely on a single static grid of radar or passive microwave observations in each orbit. LIS is a staring imager that continuously measures the optical scene, thus allowing it to record the evolution of radiance from a given flash as it develops. LIS pixels (4–5 km at the center [*Mach et al*., 2007]) otherwise compare relatively well with the PR (4.3 km at launch) and VIRS (4.22 km at launch) but are smaller than TMI pixels (37 GHz: 9.7 × 16.0 km; 85 GHz: 4.1 × 6.7 km at launch) [*Kummerow et al*., 1998]. LIS identifies illuminated pixels (events) whose brightness exceeds a dynamic background threshold at any point during its view time over a particular storm (~90 s). These events are then clustered into features known as “groups” that represent the extent of the optical impulse at a given instance. Groups that are close in space and time are combined into a single LIS “flash.” The LIS grouping algorithm that defines these features is described in detail in *Mach et al*. [2007].

An example LIS flash containing all of its subflash elements is shown in Figure 1. LIS events (yellow or grey boxes) are purposefully exaggerated for visualization purposes, and the flash center (mean latitude and longitude of all event pixels) is denoted with a black “X.” This flash occurred over Bolivia on 30 November 2001 along the flank of a multicellular convective system (Figure 1a). A typical group for this flash (i.e., by median area) is shown in Figure 1b, while ellipsoid fits around all of its 32 groups (black ellipses) are shown in Figure 1c. The footprint of the flash—or the unique spatial extent of all of its events from every group—can also be seen in Figure 1c as the yellow shaded area. This example is considerably larger than a typical LIS flash, as it was chosen for its large size to aid in visualizing its components.

To create a feature-level database of illuminated clouds by using LIS observations, it is necessary to collocate the LIS events that comprise each flash with coincident PR and TMI pixels. However, as TMI and PR are scanning instruments while LIS is a staring instrument, a single PR or TMI pixel may be collocated with multiple LIS events. A true Illuminated Cloud Feature (ICF) analog to TRMM precipitation features (PFs [*Liu et al*., 2008]) can be defined as the unique collection of PR and TMI pixels that are located with the overall flash footprint depicted as the yellow shaded region in Figure 1c. PR, TMI, and VIRS properties for each ICF are then defined by computing the maximums, minimums, means, etc. of the properties of the PR or TMI pixels contained within this collection (it should be noted that VIRS has already been collocated with the PR grid in the source data set).

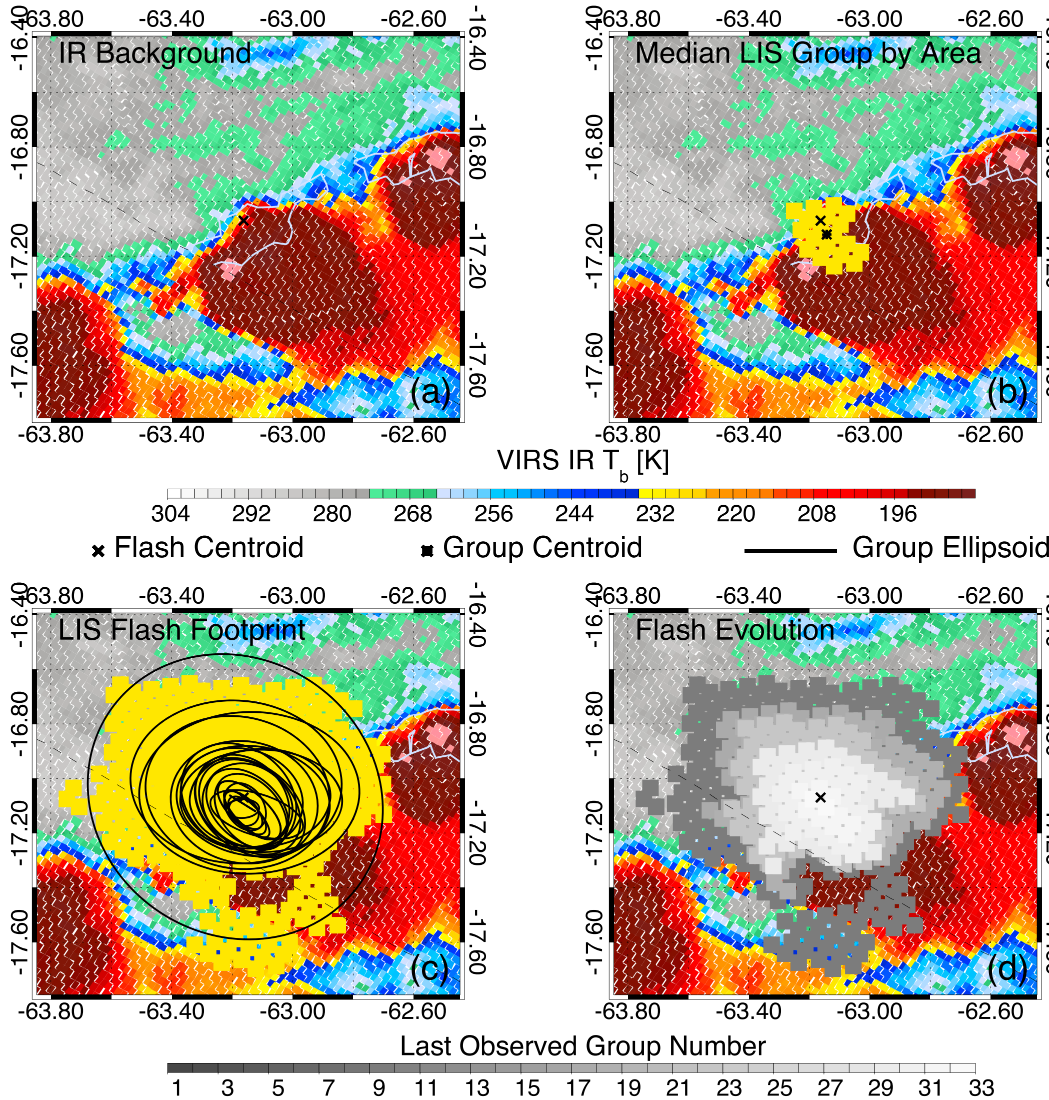

Figure 1. The elements of an example LIS flash over a (a) VIRS CH4 (10.6 μm) brightness temperature background. Included are an example (b) LIS group, (c) ellipsoid fits around all groups over the flash footprint, and (d) flash evolution shaded by the last observed group number.

The issue with this approach is that the flash footprint can be easily influenced by a small number of optically intense groups that illuminate a much larger cloud area than the rest of the flash (i.e. return strokes [*Koshak*, 2010]). This can be seen in Figure 1 by comparing the median group by size (Figure 1b) with the flash footprint (Figure 1c). Typical groups within the flash are comparable in size to the 30 dBZ at 6 km radar feature (white outline in Figure 1), and if repetition is allowed, most events are located within the cold cloud region. However, the four largest groups within the flash expand the boundaries of the flash footprint to the north and west far beyond the edge of the cold cloud. Subsequent groups after this bright pulse then decrease in area until only cold pixels are illuminated near the end of the flash (Figure 1d). These warm pixels are likely irrelevant to the flash due to the key role that ice plays in noninductive charging [*Takahashi*, 1978] and because these events are only illuminated once or in a handful of the 32 groups that constitute the flash. However, with this formulation of ICFs that looks only at the flash footprint, the cold pixels near the flash center that are illuminated by every group would be counted the same as these peripheral warm pixels.

To limit this potential source of bias, we have elected to define ICFs as the collection of PR and TMI pixels that are coincident with LIS events with repetition allowed. This change has no effect on extreme values (for example, PR echo top heights and TMI minimum brightness temperatures), but it weights measures of center (means and medians) and fractions (for example, convective fraction) by how frequently each pixel was illuminated over the course of the flash, thus prioritizing cloud regions that are consistently illuminated over those that happen to be illuminated by a particularly bright and large group. We also apply a restriction on the flashes we consider to only include those that are entirely bounded by the swaths of all four sensors (LIS, TMI, VIRS, and PR). Therefore, the flash in Figure 1 is excluded because its footprint straddles the edge of the PR swath (dashed diagonal line), the smallest of the instrument swaths at 215 km across at launch [*Kummerow et al*., 1998].

A database of ICFs is created from a subset of the TRMM record (1998 until 2011) due to computational limitations. This database includes the properties of 7 million LIS flashes and their corresponding ICFs. Of these ICFs, 33,000 lack valid VIRS measurements and 49,000 report TMI error codes and are not considered in this study. In addition to the overall properties of illuminated clouds, the ICF database also includes the properties of the cloud at specific points within the flash footprint. These points include the centroid location, the furthest event pixels by distance (i.e., overall endpoints), and the furthest event pixels in the first and last observed groups (i.e., endpoints by time). A full list of available flash and ICF properties in their native units can be found in Table 1, though not all are used in this study.

2.2. LIS Flash Length, Propagation, and Radiance Ratio

While most parameters listed in Table 1 are fairly standard in the LIS PF literature, a number of unique parameters are included that provide additional information about each flash. The first of these are two length scales: maximum event separation (elength) and maximum group separation (glength). A third length scale, the characteristic length of the flash, is calculated from the reported footprint area and defined as the hypothetical diameter a LIS flash would have if its footprint area was converted into a perfectly circular feature. The other two length scales (elength and glength) are calculated from pixel-level LIS observations. Maximum event separation is the largest horizontal distance between any two events that comprise a LIS flash and provides an observed measure of flash length. Maximum group separation, meanwhile, is the largest distance between the centroid locations of any two groups. It is sensitive to the temporal evolution of the LIS flash and provides a measure of horizontal propagation in the optical flash.

Cumulative distributions of each of these three length scales are shown in Figure 2a. The median characteristic length of all LIS flashes is 16 km, the median elength is 14 km, and the median glength is 4 km. All three lengths show some sensitivity to the day and night cycles with nighttime flashes longer than daytime flashes. The two measured length scales can also have values of 0 km. For maximum event separation, this occurs when the flash consists of a single pixel. Generally, single-pixel flashes are considered artifacts and removed by the LIS quality control algorithms, but they may also be real flashes that barely meet the criteria for detection. These flashes account for ~2% of the flashes in this sample.

In contrast, maximum group separations of 0 km indicate that the flash remains stationary over the course of its evolution. Flashes in the first glength bin in Figure 2a account for 10% of all LIS flashes including single-group flashes that have glengths of 0 by definition. However, one third of the flashes in this first bin consist of multiple groups—as many as 20—whose centroids do not differ by more than the 0.1 km bin size. At the other end of the glength distribution, the groups in roughly 5% of all flashes traverse a distance that is larger than the 14 km median observed length scale of a typical flash. These may be propagating flashes or exceptionally large flashes that do not necessarily propagate.

To identify propagating flashes properly and to ascertain whether these diurnal trends are physical, it is necessary to account for day and night differences in the background radiance. One way of doing this is to normalize each of these length scales by a similar quantity that is sensitive to the same effect. We define three ratios between the length scales that each describe an aspect of optical flash morphology:

$$\text{elongation} = \frac{\text{maximum event separation}}{\text{characteristic length}} \tag{1}$$

$$\text{characteristic propagation} = \frac{\text{maximum group separation}}{\text{characteristic length}} \tag{2}$$

$$\text{observed propagation} = \frac{\text{maximum group separation}}{\text{maximum event separation}} \tag{3}$$

Table 1. Description of LIS Flash and TRMM Illuminated Cloud Feature Database Parameters[a]

Parameter	Avail.	Unit	Description
Orbit	f		TRMM orbit number
Date	f		Date of flash
Time	f	UTC	Universal time of flash
Lat	c,d,t		Centroid latitude
Lon	c,d,t		Centroid longitude
Optical Lightning			
Area	f	km^2	Flash footprint area
Radiance	f	$\mu J\ m^{-2}\ sr^{-1}\ \mu m^{-1}$	Total flash radiance
Duration	f	s	Time between first and last event
ngroups	f		Number of groups in flash
nevents	f		Total number of event pixels in flash
minevtradiance	f	$\mu J\ m^{-2}\ sr^{-1}\ \mu m^{-1}$	Radiance of dimmest event
meanevtradiance	f	$\mu J\ m^{-2}\ sr^{-1}\ \mu m^{-1}$	Average event radiance
maxevtradiance	f	$\mu J\ m^{-2}\ sr^{-1}\ \mu m^{-1}$	Radiance of brightest event
glength	f	km	Furthest distance between groups
elength[b]	f	km	Furthest distance between events
tlength	f	km	Distance between furthest events in first/last groups
Radar			
pctinpr[c]	f	%	Fraction of flash in PR swath
ninpr	f		Number of valid collocated PR pixels
nconv	f		2A23 convective PR pixel count
nstrat	f		2A23 stratiform PR pixel count
nrconv	f		2A23 raining convective pixel count
nrstrat	f		2A23 raining stratiform pixel count
raintype	c,d,t		Mode of 2A23 rain types
minstormh	f	km	Minimum radar-derived storm height
meanstormh	f,c,b,e	km	Mean radar-derived storm height
maxstormh	f	km	Maximum radar-derived storm height
stddevstormh	f	km	Standard deviation of storm height
maxht15	f,c,d,t	km	Flash centroid 15 dBZ echo top
maxht20	f,c,d,t	km	Flash centroid 20 dBZ echo top
maxht30	f,c,d,t	km	Flash centroid 15 dBZ echo top
maxht40	f,c,d,t	km	Flash centroid 40 dBZ echo top
minnearsurfz	f	dBZ	Minimum near-surface echo
meannearsurfz	f,c,d,t	dBZ	Mean near-surface echo
maxnearsurfz	f	dBZ	Maximum near-surface echo
minnearsurfrain	f	$mm\ h^{-1}$	Minimum near-surface rain rate
meannearsurfrain	f,c,d,t	$mm\ h^{-1}$	Mean near-surface rain rate
maxnearsurfrain	f	$mm\ h^{-1}$	Maximum near-surface rain rate
stddevnearsurfrain	f	$mm\ h^{-1}$	Standard deviation of near-surface rain
Passive Microwave			
minpct85	f	K	Minimum 85 GHz PCT
meanpct85	f,c,d,t	K	Mean 37 GHz PCT
maxpct85	f	K	Maximum 85 GHz PCT
stddevpct85	f	K	Standard deviation of 85 GHz PCT
minpct37	f	K	Minimum 37 GHz PCT
meanpct37	f,c,d,t	K	Mean 37 GHz PCT
maxpct37	f	K	Maximum 37 GHz PCT
stddevpct37	f	K	Standard deviation of 37 GHz PCT
minrain2A12	f	$mm\ h^{-1}$	Minimum 2A12 rain rate
meanrain2A12	f,c,d,t	$mm\ h^{-1}$	Mean 2A12 rain rate
maxrain2A12	f	$mm\ h^{-1}$	Maximum 2A12 rain rate
stddevrain2A12	f	$mm\ h^{-1}$	Standard deviation of 2A12 rain rate
Infrared			
minvirsch4	f	K	Minimum VIRS CH4 T_b
meanvirsch4	f,c,d,t	K	Mean VIRS CH4 T_b
maxvirsch4	f	K	Maximum VIRS CH4 T_b
stddevvirsch4	f	K	Standard deviation of VIRS CH4 T_b

[a]Parameters may be available at the flash centroid location (c), two furthest event pixels (endpoints) by distance (d), two furthest event pixels (endpoints) by time (t), or for bulk properties of the whole cloud illuminated by the flash (f).
[b]Only available for a subset of all flashes.
[c]Always 100% in this study.

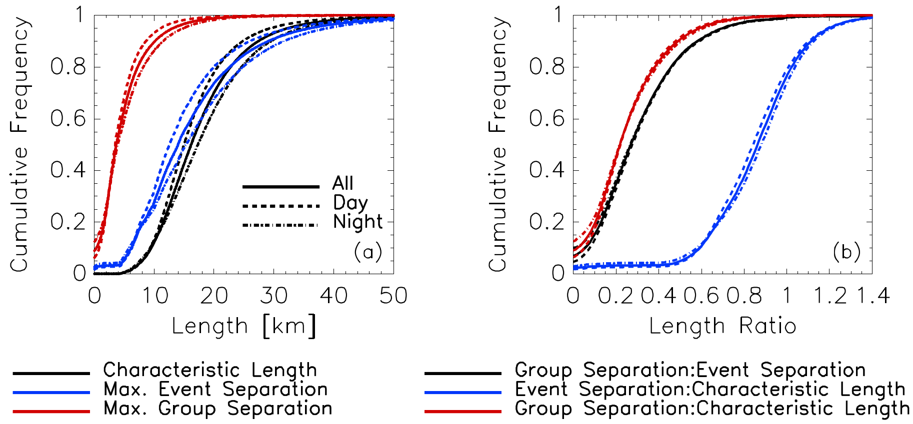

Figure 2. Cumulative distribution functions (CDFs) of (a) LIS length scales and the (b) ratios between them.

The ratio of maximum event separation to characteristic length in equation (1) provides an observed measure of flash elongation by comparing the measured distance across the flash against the diameter of a perfectly circular flash with the same area. The remaining two ratios provide measures of horizontal flash propagation normalized by flash size. We define the first of these as characteristic propagation (equation (2)) as it compares the maximum spacing of LIS groups against the size of an ideal circular flash. Similarly, we denote the second as observed propagation (equation (3)) since it uses the measured maximum length of the flash footprint for this purpose.

These metrics are preliminary and, as such, are subject to certain caveats that affect how they are interpreted. Future work will refine our measures of elongation and propagation and compare them to ground-based measurements. The first caveat is that one would expect a circular flash to have a ratio of maximum event separation:characteristic length of 1. However, maximum event separation is calculated from the event pixel center, while characteristic length (and flash area) includes whole pixels in its derivation. Because of this, a circular flash will have an elongation considerably less than 1 that depends on the size of the flash. For this reason, it may be attractive to define propagating flashes based on the observed propagation that does not mix data types in its formulation. The issue with this approach, however, is that the definition of observed propagation relies on just four points within the flash footprint (two event centers and two group centers) and therefore is likely more prone to bias. The characteristic propagation ratio, on the other hand, takes into account the entire footprint of the flash and should be generally more robust. Using these parameters, we identify elongated and propagating flashes as follows:

$$\frac{\text{elongation} \leq 1 \mid \text{not elongated}}{\text{elongation} > 1 \mid \text{elongated}} \tag{4}$$

$$\frac{\text{characteristic propagation} \leq 0.5 \mid \text{not propagating}}{\text{characteristic propagation} > 0.5 \mid \text{propagating}} \tag{5}$$

These thresholds are defined empirically through the analysis of 100 flash cases. They are chosen to eliminate flashes where propagation and elongation are not apparent to an observer. An elongation factor exceeding 1 means that the maximum distance between event centers exceeds the diameter of a circular flash with the same area, while a characteristic propagation exceeding 0.5 indicates that the maximum separation between group centers exceeds its radius. Though there is considerable overlap between these two groups, these definitions of elongated and propagating flashes are considered independently from one another. This is necessary because elongated flashes may not be observed to propagate, while propagating flashes in some cases may not appear to be elongated.

Finally, it is important to define a parameter that defines the radiative intensity ("brightness") of the flash that can be compared against its apparent footprint area in a radiative transfer framework. While Mie scattering involves complex calculations that are best suited for Monte Carlo experiments [see *Thomason and Krider*, 1982; *Koshak et al.*, 1994; *Light et al.*, 2001], it is possible to make some basic deductions that can be tested

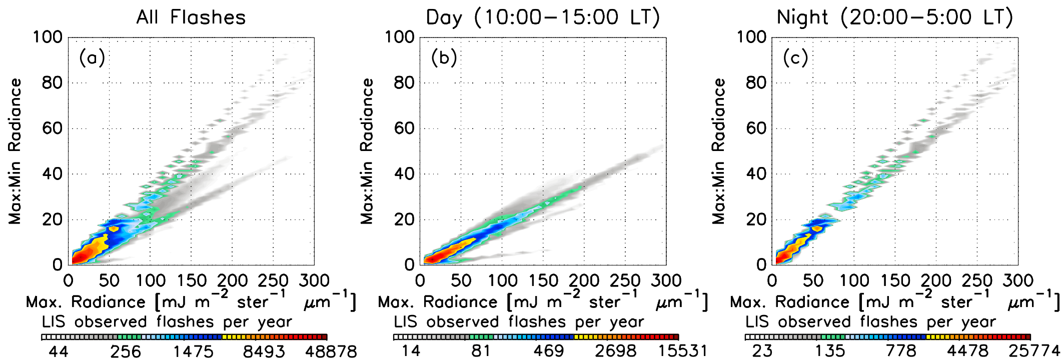

Figure 3. Two-dimensional histograms of maximum radiance and maximum to minimum radiance ratio for all (a) flashes, (b) daytime flashes, and (c) nighttime flashes.

with the LIS measurements. For example, we know that there is a background threshold that defines the minimum radiance that would be considered a flash [*Mach et al*., 2007]. Therefore, the lateral boundary of the LIS flash is determined by where the optical radiance of the scene crosses this threshold. If the radiative intensity of the flash was increased but nothing else changed, it would be reasonable to expect the radiance pattern [i.e., *Light et al*., 2001, plate 2] to be amplified, adding at least some photons in a Monte Carlo sense to each grid point. With this additional radiance, grid points along the periphery of the flash that previously fell short of the minimum LIS threshold would now be detected and incorporated into the flash, causing its footprint to increase in size.

As a result, we would expect to find some relationship between the size of observed LIS flashes and their maximum brightness relative to the dynamic background. This relative measure of radiance may be expressed as either a quotient or a difference of maximum and minimum observed event radiances. The choice of which parameter to use turns out to be largely moot, as maximum event radiance varies across a range that is 45 times greater than the range of minimum event radiance. As a result, both parameters are highly correlated with maximum event radiance ($r = 0.9996$ for differential radiance, $r = 0.966$ for radiance ratio) and with each other ($r = 0.963$). We elect to choose radiance ratio over differential radiance because only radiance ratio provides unique information about the brightness of the flash that is not contained within the maximum event radiance. Furthermore, the ratio between the brightest and dimmest events if the flash is a simple quantity to contextualize unlike an absolute radiance. The differences in these parameters come from how radiance ratio responds to the dynamic LIS background radiance threshold that determines the minimum event radiance in a flash. This can be seen in the two-dimensional histograms in Figure 3 between radiance ratio and maximum event radiance. The distributions take the shape of rays emanating from the origin (Figure 3a) that are a superposition of the distributions for each of the discrete thresholds employed. This results in a different collection of rays for day (Figure 3b) and night (Figure 3c) as the sensitivity of the instrument changes. The diurnal sensitivity of radiance ratio is also an advantage over differential radiance. As differential radiance is essentially identical to maximum event radiance, it would remain nearly constant if the same flash were observed both at night and during the day. Flash area and radiance ratio, on the other hand, would both increase in the nocturnal case due to the increased instrument sensitivity.

3. Results

Since LIS is a total lightning detection system that observes both intracloud and cloud-to-ground flashes, it can be expected that the flashes observed by LIS will be highly diverse with considerably different sets of optical properties among them, even before scattering in the cloud is considered. The optical properties of LIS flashes can be influenced by the radiative intensity of the flash, the structure of the discharge, and the scattering properties of the illuminated cloud. In the following sections, a survey of LIS flashes will be performed (section 3.1), variations in optical properties will be considered independent of the surrounding cloud (section 3.2), the properties of illuminated clouds will be examined (section 3.3), and finally, land and ocean trends in optical lightning characteristics will be assessed for flashes that illuminate otherwise similar clouds (section 3.4).

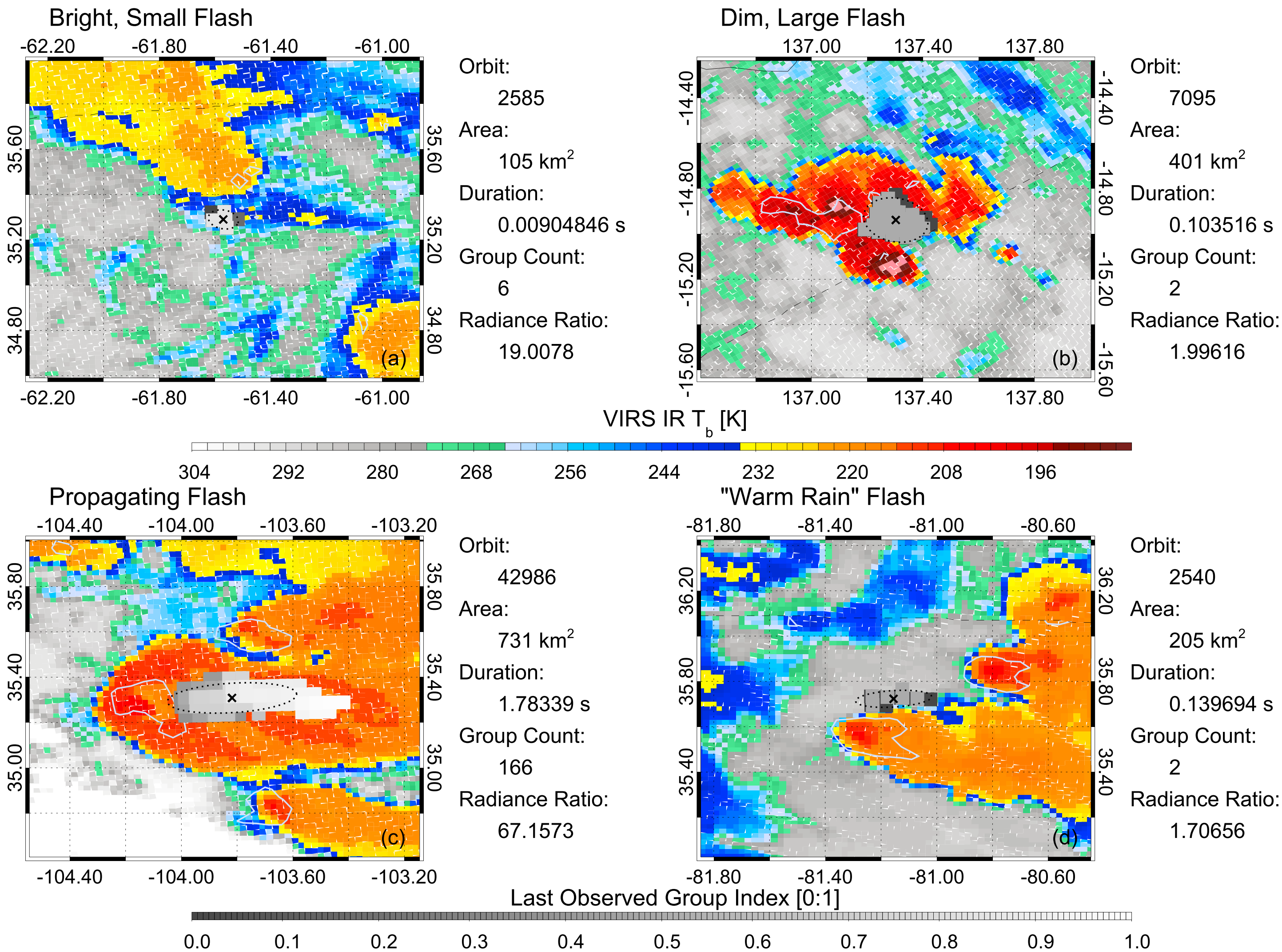

Figure 4. (a–d) Examples of the evolution of four LIS flashes with distinct sets of properties. As in Figure 1d but with last group number normalized to 1, ellipsoid fits around the flash footprint added (dashed lines) and regions with PR echoes >30 dBZ at 6 km outlined in white.

3.1. Survey of Exceptional and Propagating LIS Flashes

A first step to examining the problem of radiative transfer for optical flashes is to analyze just how different optical flashes can appear from one another. Four examples of LIS flashes are shown in Figure 4. The first example (Figure 4a) is a case of a flash that is particularly bright (radiance ratio: 19) with a small area (105 km^2) that was observed on 10 May 1998. It consists of six groups in 9 ms for a total of 19 events and is located near the edge of a cloud with IR T_bs around 250 K. PR and TMI observations indicate that the flash occurred in a weak convective cloud region with low echo top heights (< ~7 km) compared to the rest of the storm (>12 km). Therefore, a lack of cloud optical depth for scattering to occur may have contributed to its inability to illuminate a larger area.

In contrast to the example flash in Figure 4a, the flash in Figure 4b is large (405 km^2) and dim (radianceratio: 2). Observed on the evening of 20 February 1999 was a nocturnal case that consisted of just two groups in 100 ms containing a total of 49 event pixels. It was coincident with a convective anvil region that had cold (<200 K) IR T_bs but no accompanying PR echoes. If this is an example of an anvil crawler along the base of the cloud, then the intervening anvil may have blocked much of the radiance from reaching LIS, resulting in the large area but dim radiance that was observed. Moreover, with the peak radiance so close to the threshold value, this flash would not likely be detected if it had occurred during the day.

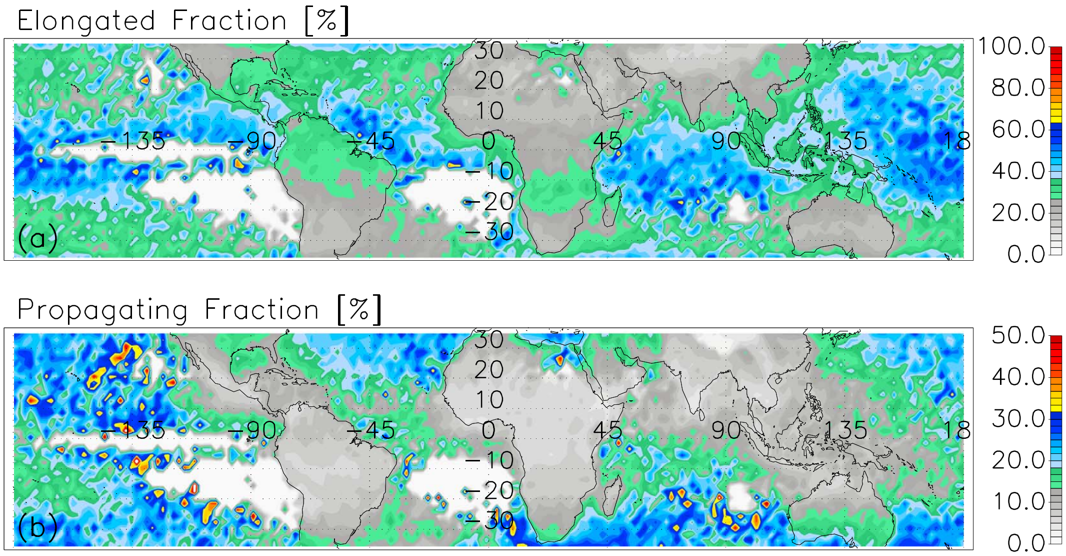

Figure 5. Fractions of (a) elongated flashes and (b) propagating flashes across the TRMM domain.

The third flash in Figure 4c is an example of a propagating flash observed on 31 May 2005. It consists of 166 unique groups that begin illuminating the edge of a convective cell (white outline) and then progress deeper into the anvil as the flash evolves over its 1.8 s duration. The flash achieved a radiance ratio of 67 due to a single large group that was possibly a return stroke. During the period in which the flash was propagating, the group radiance ratios were similar to the flash in Figure 4b with an average ratio of 2. These dim structures are difficult for LIS to resolve compared to radiant strokes, limiting its utility as a lightning mapper. However, unlike the previous example, this flash was observed during the day (14:00 LT) and propagation in nocturnal cases would be better resolved.

The final example in Figure 4 uses the ICF database to identify a case of a "warm rain" flash that only illuminates VIRS pixels above freezing. This flash was observed on 7 May 1998 and happens to be elongated but does not propagate. It contains two groups over the course of 140 ms. This flash and the other warm rain cases that were considered for this study were all immediately adjacent to cold clouds and are likely the result of parallax or blocking by intervening ice clouds in scenarios similar to Figure 4b. If there are warm rain flashes in the LIS record that are not artifacts, no obvious examples have been identified in the ICF database.

Though the example flash in Figure 4d would be considered an elongated flash, it is an exceptional case. Propagating flashes like the example in Figure 4c also take on an elongated appearance, but most elongated flashes resemble the example flash in Figure 1 with overlapping elliptical groups that do not propagate in time. Highly elongated flashes that are not observed to propagate may still be examples of propagating flashes, however, if the groups propagate across the cloud on time scales that are shorter than LIS can resolve (~2 ms)—for example, in cases of re-illumination along existing channels.

Global distributions of the fraction of elongated or propagating flashes are shown in Figure 5. Overall, 12% of LIS flashes in the ICF database propagate, while 24% of all flashes are elongated. Both types of flashes are more common offshore than over land. Propagating flashes account for 10% of land-based flashes and 16% of oceanic flashes, while 22% of flashes over land and 31% of flashes offshore are elongated. Higher propagating and elongated flash fractions can be found in certain parts of the TRMM domain, however. Elongated flash fractions are greatest near the equator and account for 50–60% of all LIS flashes in many oceanic regions in the deep tropics. On the other hand, propagating flash fractions are greatest poleward of $>20°$ latitude and in the tropical eastern Pacific, where they account for 20–30% of all lightning.

3.2. Optical Properties of Lightning Flashes

One of the complications that the radiative transfer aspect of optical flashes introduces is that the observed flash properties are not entirely independent from one another. The sensitivity of flash area to radiance ratio has been mentioned and leads to a correlation coefficient of 0.64 between the two parameters. In other

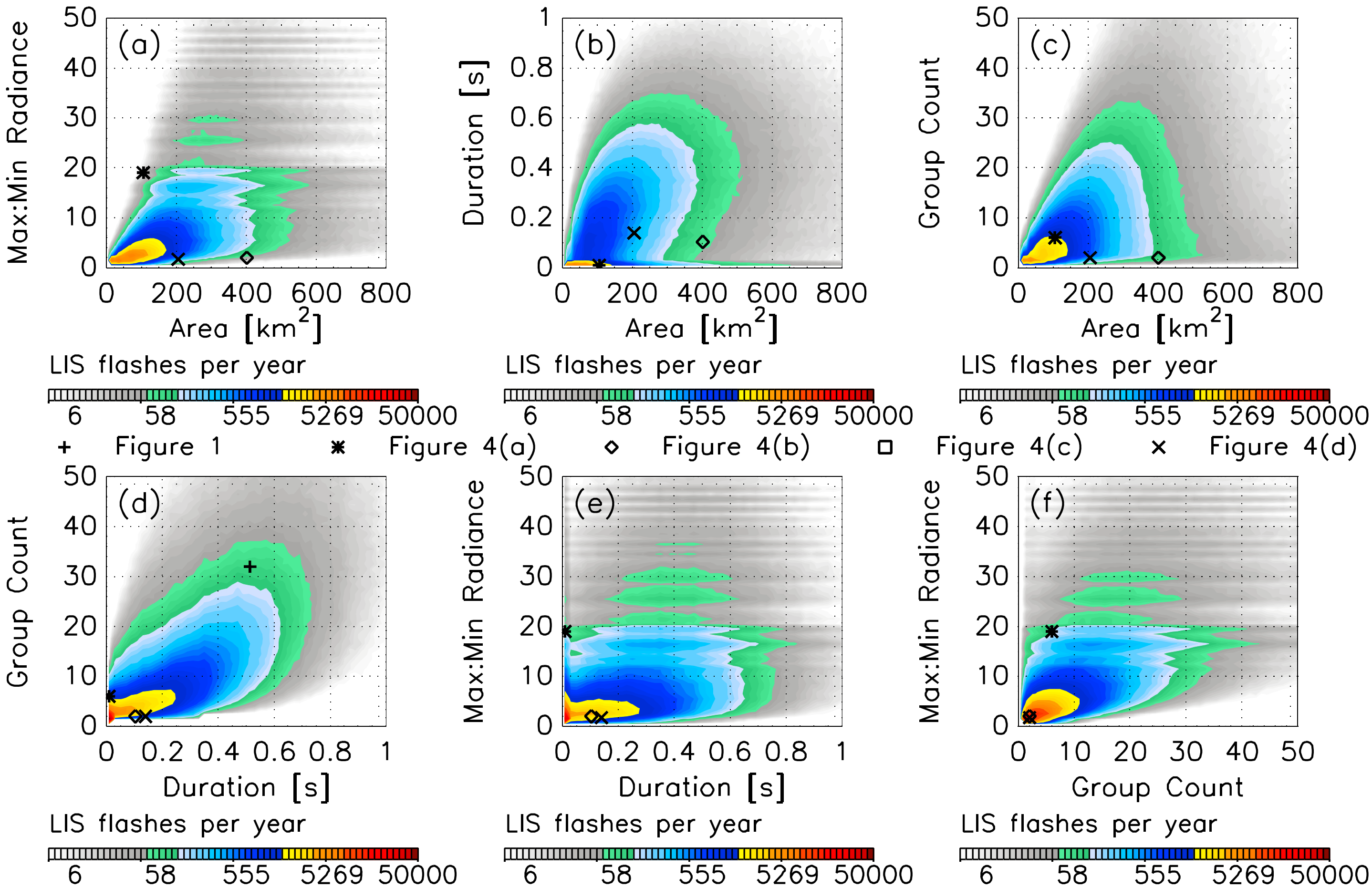

Figure 6. Two-dimensional histograms of (a) flash area and radiance ratio, (b) flash area and duration, (c) flash area and group count, (d) flash duration and group count, (e) flash duration and radiance ratio, and (f) flash group count and radiance ratio.

words, a simple linear model involving radiance ratio is sufficient to explain 41% of the observed variation in flash footprint area, while factors that would not be represented in such a model (i.e., differences in scattering and breakdown structure) may result in the remaining 59%. Two-dimensional histograms of flash area, radiance ratio, duration, and group count are shown in Figure 6 that demonstrate how each property relates to the others. The properties of the example flashes in Figures 1 and 4 are overlain. Each set of parameters hints at a positive correlation with coefficients that range from 0.38 between duration and either area or radiance ratio (Figures 6b and 6e) to 0.7 between duration and group count.

A unique feature of some of these distributions is the presence of well-confined boundaries that indicate limits on the sets of optical properties that flashes may attain. For example, while the upper boundary of the distribution between duration and group count (Figure 6d) fades gradually to grey with additional groups, the lower boundary of this distribution is constrained to 1 at 0 s and 2 between 0 s and 0.3 s. In this example, the "hard" boundary is due to a systematic limitation in the methodology: flashes cannot have less than one group, and we require two or more groups to define a finite duration. However, the lines that describe the minimum size of a flash with a given radiance ratio (Figure 6a), duration (Figure 6b), or group count (Figure 6c) do not have obvious methodological explanations.

Three of the four example flashes in Figure 4 fall along such a boundary in Figure 6a: two along the lower boundary that denotes the dimmest flashes for a flash of a given footprint area and one along the left boundary that denotes the smallest flashes for a given radiance ratio. The linear nature of both boundaries in Figure 6a is reinforced by the fact that replacing the linear fit that with a polynomial repression decreases the correlation coefficient between the two parameters. This distribution is presented for all regions—land and ocean—and all hours because the terrain and diurnal sensitivity of LIS has only a marginal effect on its shape. Despite ocean regions containing larger and brighter flashes, on average, the land and ocean distributions are bounded by the same “wedge” shape.

One way to make sense of this trend is to entertain the idea that the distributions in Figure 6 are a superposition of solutions to the radiative transfer problem for all possible scenarios: every flash type, cloud type, background radiance, flash altitude, etc. In any one of these scenarios, as radiant energy is added to the flash, the radiance pattern would be amplified through scattering, resulting in a larger footprint area that LIS can detect. How the flash would grow depends on the scenario, and radiative transfer modeling would be required to distinguish the curve describing this growth from the possible solutions across the domain of Figure 6a. We can constrain the bounds of these curves, however, by using the boundaries of the distribution. If we assume that the linear nature of the boundaries implies an inverse-square law that can be adequately modeled with a linear fit that passes through (0,0), the relationship between the radiance of a flash and its illuminated area would take the form

$$\frac{I_{\text{max}}}{I_{\text{min}}} = \varepsilon^* A \tag{6}$$

where the ratio of the radiance of the brightest event (I_{max}) to the radiance of the dimmest event (I_{min}) in the flash is directly proportional to flash area. The slopes of the boundary curves indicate that the coefficient ε varies between 0.004 km^{-2} (lower boundary) and 0.2 km^{-2} (upper boundary) for all scenarios of LIS flashes. Conversely, a flash adds anywhere between 5 km^2 and 250 km^2 to its footprint for every factor its brightest event attains above the background radiance threshold.

Multivariate trends are explored in Figure 7 by computing the mean optical properties of flashes in this parameter space. Six parameters are considered: the number of hours from local noon (related to LIS sensitivity; Figure 7a), group count (Figure 7b), total radiance (Figure 7c), duration (Figure 7d), the mean optical power over the duration of the flash (Figure 7e), and the ratio of maximum group separation to characteristic length (normalized propagation; Figure 7f). Mean optical power is a derived parameter introduced by *Peterson and Liu* [2013] and is defined as total radiance divided by the product of flash area and duration. It provides a measure of the sustained brightness of the optical flash that scales with the size of the flash and group frequency. As in *Peterson and Liu* [2013], we do not define a mean optical power for single-group flashes. Small flashes and particularly bright flashes along the left boundary of the distribution, like the example in Figure 4 a, are likely to occur closer to noon ($<$4 h) than larger flashes (~6 h). Horizontal streaking can also be noted in Figure 7a at radiance ratios of 20–24, 27, 29, 33, etc. This could be the result of sensor saturation [*Koshak et al.*, 2000].

Of the five remaining parameters shown in Figure 7, four (total radiance, group count, duration, and normalized propagation) increase with both increasing area and radiance ratio, but not necessarily each variable, individually. For extreme cases in Figure 7d where flashes have areas of 300 km^2, radiance ratios of 15 but are on average of similar duration, flashes are extremely bright (radiance ratio: 45) with the same area or they are exceptionally large (700 km^2) with the same brightness. However, flashes that are both bright and large (radiance ratio: 45, area: 700 km^2) last 0.2 s longer, on average, than any of these other combinations. By contrast, mean optical power (Figure 7e) is high along the left boundary, drops below 0.75 $\text{W m}^{-2}\ \text{sr}^{-1}\ \mu\text{m}^{-1}$ with flash area, and then plateaus around 0.4 $\text{W m}{-}^{2}\ \text{sr}^{-1}\ \mu\text{m}^{-1}$ across a range of flash areas and radiance ratios. These flashes are bright and small like the example in Figure 4a.

The distribution of average normalized propagation is unique in another way: it is the only distribution that includes portions of parameter space that would lead to both positive and negative correlation coefficients. Though mean group characteristic lengths increase monotonically with radiance ratio (Figure 7f), characteristic propagation begins to increase with increasing flash area, reaches a maximum value that depends on radiance ratio, and then decreases as flash area continues to increase. For dim flashes, this maximum is reached at 300 km^2 (~20 km characteristic length), while for brighter flashes it is closer to 500 km^2.

3.3. Properties of Illuminated Cloud Regions

Until this point, the properties of the cloud region have been treated as an unknown quantity. This section aims to incorporate the properties of the illuminated clouds in the ICF database into the discussion of optical flashes. To gain a sense of perspective of how illuminated clouds relate to cloud features derived from satellite measurements, ICFs are compared to RPF thunderstorms identified by using TRMM PR measurements

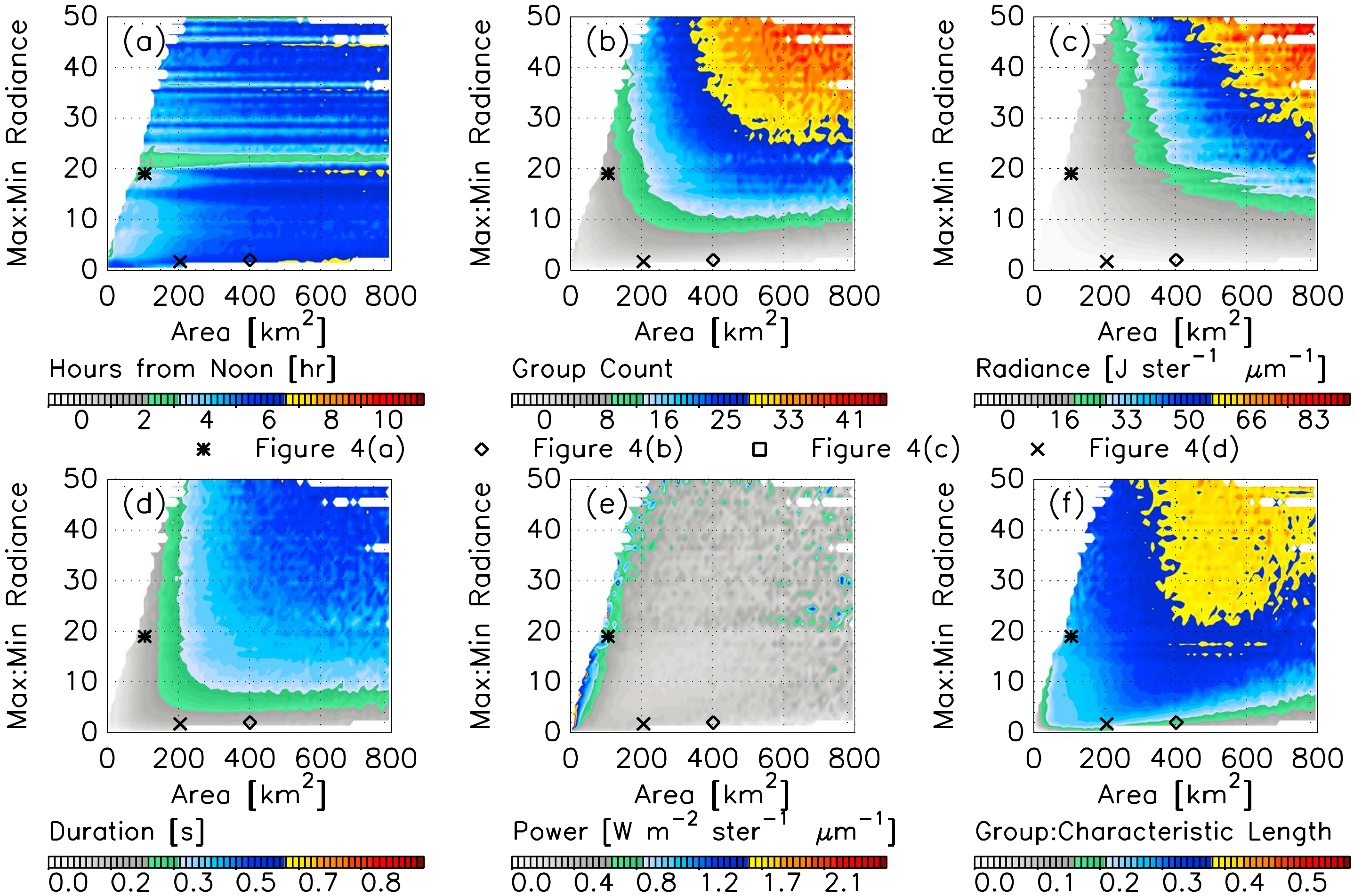

Figure 7. Mean hours from (a) noon, (b) groups per flash, (c) total radiance, (d) duration, (e) mean optical power, and (f) maximum group separation:characteristic length for flashes with different combinations of area and radiance ratio.

(RPFs with LIS flash centroids located within their boundaries). The median and 90th percentile properties of RPFs and ICFs are listed in Table 3. The ocean is divided into two regions separating "coastal" waters from the "open ocean" (abbreviated ocean) for consistency with *Peterson and Liu* [2013]. The boundary between these ocean regions is placed at 1000 km offshore. As indicated in the table, RPF thunderstorms are typically on the order of 1000 km^2 (median) to 10,000 km^2 (90th percentile), encompassing the entire convective systems or even mesoscale convective systems (MCSs). By contrast, ICFs are quite small because they bound individual lightning flashes, usually only on the order of one tenth the size of a typical RPF. Land and ocean contrasts in storm properties can be noted for each type of feature. For RPFs, oceanic features are 4 times larger than features over land, while ICFs are twice as large. Despite the differences in spatial extents between ICFs and RPFs, passive microwave minimum polarization-corrected temperatures (PCTs [*Spencer et al.*, 1989]) are typically comparable. PCTs are sensitive to cloud ice within the column [*Vivekanandan et al.*, 1991], with the longer wavelength at 37 GHz more sensitive to larger ice particles like hail [*Cecil*, 2009]. Similarities in the microwave signals between ICFs and RPFs imply that illuminated clouds are typically coincident with strong convection, which is consistent with the higher flash rates in those storm regions.

The issue of tying lightning flashes to a single pixel noted previously can be observed in Table 2. Comparing the mean and minimum PCTs for typical ICFs (median), an 8 K (land) to 9 K (coast) difference can be noted at 37 GHz, while at 85 GHz this difference is as large as 38 K (land) to 47 K (coast). Despite their small size (on the order of 100 km^2), it appears that ICFs often occur along PCT gradients where the center pixel may not always be representative of the entire illuminated cloud. Strong microwave gradients also imply gradients in the quasi-steady state electric field following the retrieval algorithm presented in *Peterson et al.* [2015]. Flash

Table 2. Summary of RPF Thunderstorm and ICF Properties[a]

		RPF Thunderstorms		Illuminated Cloud Regions	
		Median	90%	Median	90%
Area (km^2)	land	997	9,177	165	482
	coast	1,846	21,367	216	643
	ocean	**4,212**	**35,470**	**231**	**705**
Min. 85 GHz PCT (K)	land	201	131	190	120
	coast	181	124	**178**	**112**
	ocean	**170**	**122**	180	117
Mean 85 GHz PCT (K)	land			228	160
	coast			225	**156**
	ocean			**224**	161
Min. 37 GHz PCT (K)	land	265	238	255	216
	coast	262	238	**253**	**213**
	ocean	**258**	238	255	223
Mean 37 GHz PCT (K)	land			263	231
	coast			**262**	**230**
	ocean			**262**	236
Min. VIRS IR (K)	land	208	188	**204**	**186**
	coast	**203**	**186**	**204**	**186**
	ocean	208	188	212	194
Mean VIRS IR (K)	land			**214**	**191**
	coast			215	193
	ocean			221	201
Max. storm height (km)	land			**12.1**	**15.7**
	coast			12.0	15.6
	ocean			10.3	14.1
Mean storm height (km)	land			**9.0**	**13.8**
	coast			8.5	13.4
	ocean			7.5	11.6
15 dBZ echo top height (km)	land	11.5	**15.0**	**13.0**	**16.0**
	coast	**12.0**	**15.0**	**13.0**	**16.0**
	ocean	11.5	14.0	11.2	15.0
20 dBZ echo top height (km)	land	11.5	**15.0**	**12.5**	**16.0**
	coast	**12.0**	**15.0**	12.2	**16.0**
	ocean	11.2	14.0	10.5	14.0
30 dBZ echo top height (km)	land	**9.0**	**13.0**	**9.8**	**14.0**
	coast	8.8	12.0	9.5	**14.0**
	ocean	8.5	11.0	8.0	12.0
40 dBZ echo top height (km)	land	**6.0**	**8.0**	**6.5**	**10.0**
	coast	5.8	7.0	6.0	9.0
	ocean	5.2	6.0	5.2	8.0
Max. near-surface rain (mm h^{-1})	land	29.1	72.0	21.9	57.0
	coast	37.0	89.0	**25.5**	**68.0**
	ocean	**43.1**	**93.0**	25.0	66.0
Mean near-surface rain (mm h^{-1})	land			7.9	25.0
	coast			**8.2**	**27.0**
	ocean			7.4	25.0
Convective fraction (%)	land	**52.3**	**79.0**	**79.2**	100
	coast	46.9	75.0	74.2	100
	ocean	34.0	61.0	62.9	100
Stratiform fraction (%)	land	46.8	84.3	4.5	51.0
	coast	51.9	83.0	8.4	58.0
	ocean	**64.5**	**85.0**	**15.1**	**70.0**

[a]Extreme values for each category are in bold.

propagation is linked to the potential gradient of the cloud where the flash is initiated [*Vonnegut*, 1983; *Coleman et al.*, 2008]. Though the current *Peterson et al.* [2015] algorithm is built for an observer above an electrified cloud of interest, it may still be possible to link observed LIS flash propagation to microwave-derived electric field vectors in the future.

ICFs are also associated with strong convection in PR measurements with echo top heights consistently higher than their RPF counterparts. Additionally, while the median RPF reflectivity profile favors higher 15 and 20 dBZ echo top heights in coastal regions and taller 30 and 40 dBZ echo top heights over land, the median ICF radar profiles are exclusively higher over land than either of the two ocean regions. Radar-derived maximum near-surface rain rates and stratiform fractions are also higher for oceanic thunderstorms than their land-based counterparts and favor RPFs over ICFs. These differences are likely due to the competing effects of differing storm structure, size differences between RPFs and ICFs, and bias from high flash rate storms in the ICF statistics (a single high flash rate RPF may produce on the order of 10^2 ICFs).

As with the optical properties in Figure 7, we can also compute the mean VIRS, TMI, and PR properties of the ICFs across the parameter space of Figure 6a to get a sense for what types of clouds are associated with each combination of flash area and radiance ratio. Distributions for nine different ICF parameters are shown in Figure 8: minimum (Figure 9a), mean (Figure 8b), and maximum (Figure 8c) infrared brightness temperature; minimum (Figure 8d), mean (Figure 8e), and maximum (Figure 8f) PR maximum storm height; and the raining fraction for convective and stratiform pixels (Figure 8g), the convective pixel fraction (Figure 8h), and the stratiform pixel fraction (Figure 8i).

In terms of infrared brightness temperature, most combinations in parameter space correspond to cloud regions with infrared brightness temperatures around 200 K, but that often include VIRS pixels that are 30–50 K warmer. A distinct feature of these distributions is that small and bright flashes like the example in Figure 4a along the left boundary of the distribution are considerably warmer than other flash types. These are still cold clouds (~230–250 K) but with relatively high cloud top temperatures (low heights) for lightning-producing storms (i.e., Table 2). By contrast, large and dim flashes that fall along the lower boundary of the distribution not only illuminate cloud regions whose infrared brightness temperatures are typical of thunderstorms, overall, but also usually include some colder pixels that are closer to the 90th percentile minimum brightness temperatures in Table 2. Larger flashes are also prone to illuminating much warmer pixels like the flash in Figure 1, while small and dim flashes near the origin occur in cloud regions that are fairly homogeneous with only slight differences between typical minimum, mean, and maximum brightness temperatures.

PR-based estimates of ICF storm top heights are shown in the second row of Figure 8. As before, left boundary flashes are associated with shallow clouds that have mean and maximum storm heights around 6 km. However, lower boundary flashes often include radar pixels without detected radar echoes corresponding to storm heights of 0 km (Figure 8d). Lower boundary flashes are also associated with much lower mean storm heights than elsewhere in the distribution. Despite this, lower boundary flashes typically illuminate at least some areas of strong convection (Figure 8f). Cold VIRS brightness temperatures without accompanying radar echoes detected by the PR are indicative of anvil flashes like the example in Figure 4b.

The final set of ICF properties in Figure 8 describes the raining and convective and stratiform fractions of each illuminated cloud. Once more, the boundaries of the distributions stand out. Left boundary flashes are prone to illuminate regions of nonraining clouds (Figure 8g) and cloud regions that cannot be characterized as convective (Figure 8h) or stratiform regions (Figure 8i). Dim lower boundary flashes also typically contain nonraining cloud regions but have higher stratiform fractions than their small and bright counterparts. Intermediate categories between these two extremes usually are entirely encompassed by raining clouds (and therefore RPFs) that are either primarily convective (small ICFs) or mixed convective and stratiform (large ICFs). Lightning flashes that only illuminate stratiform pixels are also observed and make up 2.4% of all LIS flashes or 43% of all stratiform flashes [*Peterson and Liu*, 2011].

These results indicate that (1) the properties of ICFs—not just RPFs—often differ between land and ocean regions and (2) flashes with different sets of optical properties are associated with different types of clouds. Therefore, the concerns of *Boccippio et al*. [2000] that oceanic flashes may not be truly more energetic than flashes over land were justified. If we are to distinguish fundamental differences in land and ocean lightning in terms of energetics and structure using the optical data, it is necessary to account for these differences in illuminated clouds.

3.4. Illumination of Similar Clouds

A robust method for determining whether optical oceanic flashes are truly more energetic would require coincident measurements of cloud optical depth and radiative transfer modeling. However, there is a simpler

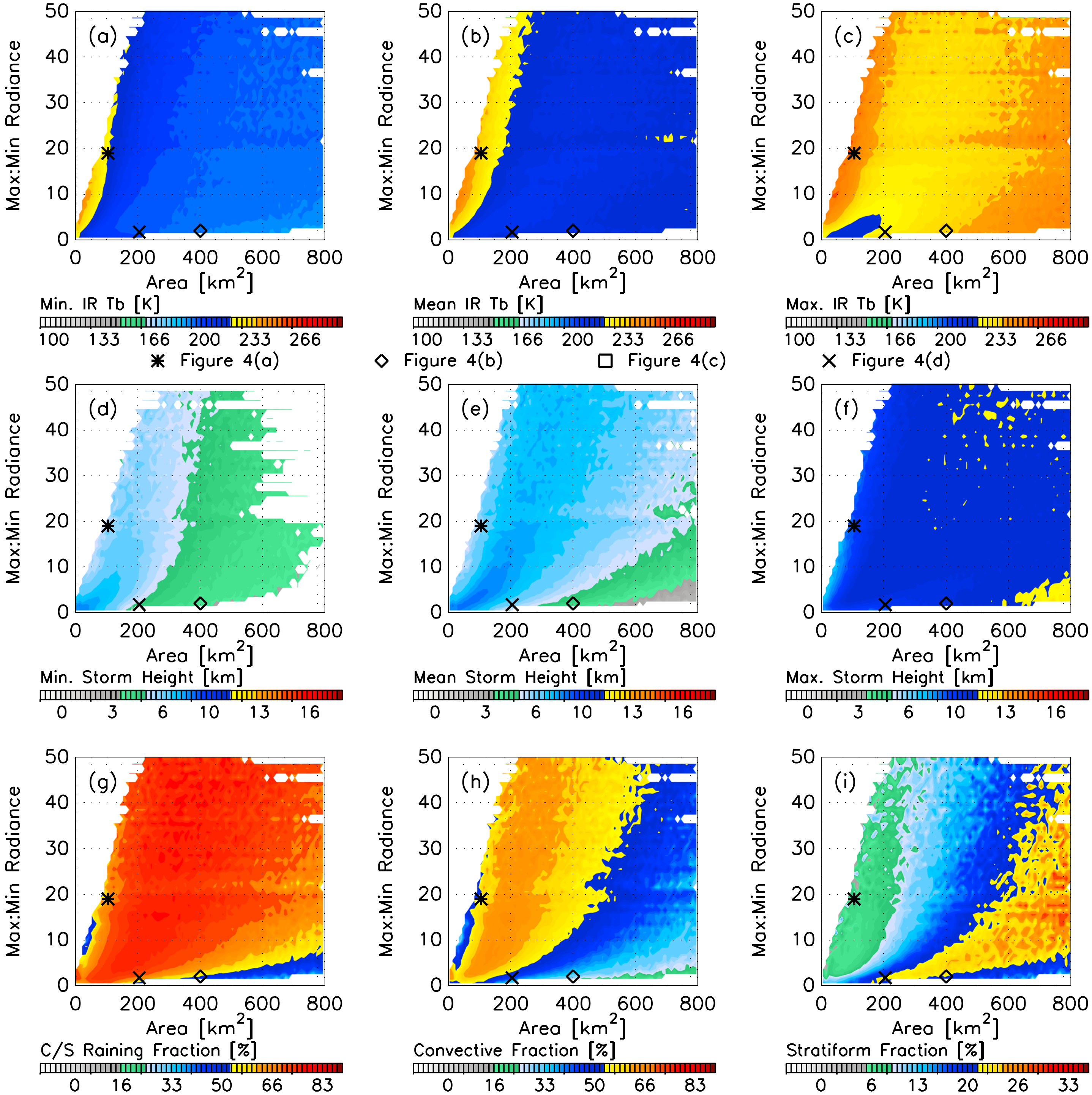

Figure 8. Mean ICF (a) minimum, (b) mean, and (c) maximum infrared brightness temperature; (d) minimum, (e) mean, and (f) maximum PR storm height; and convective and stratiform pixel (g) raining fraction, (h) convective pixel fraction, and (i) stratiform pixel fraction of clouds illuminated by flashes with various combinations of footprint area and radiance ratio.

approach that takes advantage of the large size of the ICF database to bootstrap an answer. If we assume that differences in scattering between clouds are related to their distributions of hydrometeors, we would expect that clouds with similar passive microwave, radar, and infrared properties would be illuminated in the same manner regardless of whether they occurred onshore or over the ocean. Therefore, if nearly identical ICFs are observed under the same background radiance and the flashes are still larger and brighter over the ocean,

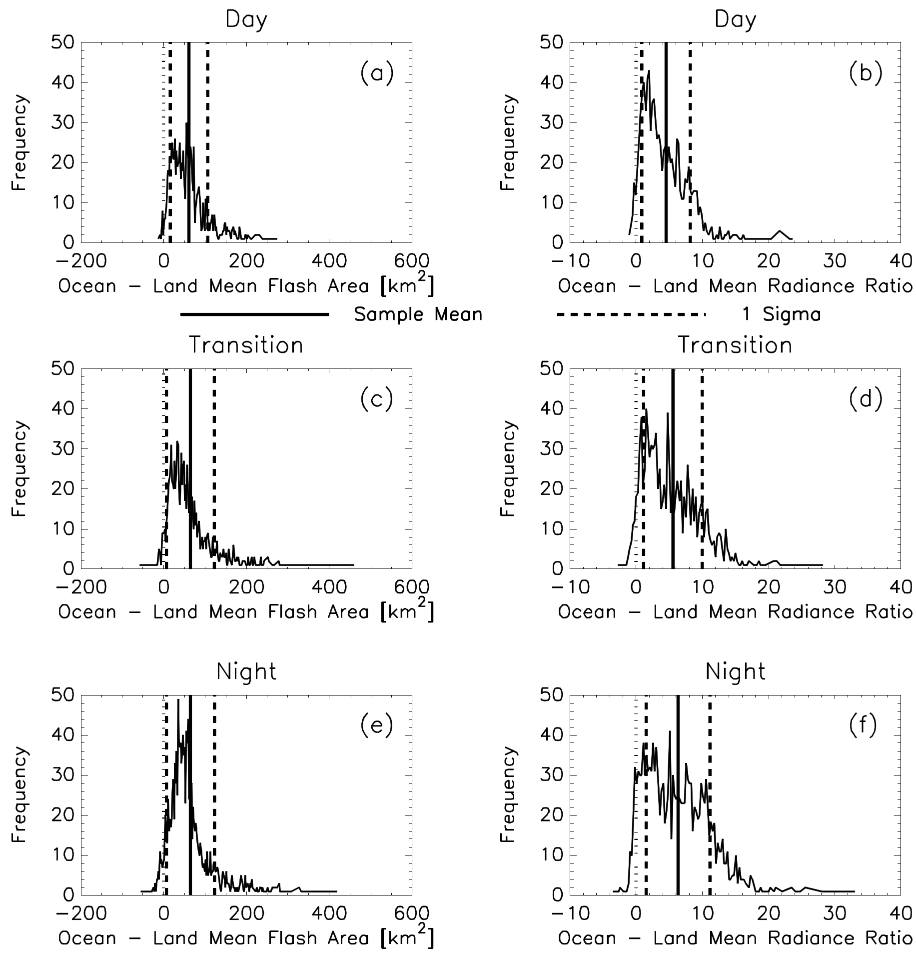

Figure 9. Histograms of the difference in (a, c and e) flash area and (b, d, and f) radiance ratio between land and ocean flashes in otherwise similar clouds observed under daytime (8:00–16:00; Figures 9a and 9b), transition (5:00–8:00 or 16:00–19:00; Figures 9c and 9d), and nighttime (0:00–5:00 or 19:00–24:00; Figures 9e and 9f) background radiance conditions.

then the trends noted in literature should be indicative of a physical difference in flash energetics or structure rather than due to different scattering properties.

First, the statistical significance of land and ocean differences in flash properties is determined in Table 3. A two-sample Student's *t* test is performed on the optical properties of land and ocean (coastal and open ocean) flashes. With the large size of the ICF database, *T* score of 3.09 is required for statistical significance at the $p < 0.001$ level. Based on this threshold, all of the parameters listed—area, radiance ratio, duration, groups per flash, propagation, total radiance, and mean optical power—are significantly greater over the ocean than over land for all three diurnal sensitivity regimes.

However, this test includes all cloud types. A simple experiment is designed that identifies similar clouds in the ICF database. Distinct classes of clouds are constructed based on specific combinations of their VIRS, PR, and TMI properties. Illuminated clouds whose properties fall within specified tolerances (10 K for brightness temperatures from 50 to 300 K, 1 km for heights from 0 to 20 km, 20% for fractions) for all parameters chosen are considered to be similar. Initially, eight parameters were chosen as degrees of freedom for the experiment: minimum 85 GHz PCT, mean 85 GHz PCT, radar storm height, maximum 20 dBZ echo top height, maximum 30 dBZ echo top height, maximum 40 dBZ echo top height, convective pixel fraction, and diurnal LIS sensitivity (day, dusk/dawn, night). This produced 3 billion unique combinations of illuminated clouds that far surpassed the 7 million flashes, and sample size became an issue for even sets of properties that are common for thunderstorms. The continuous lightning observations that will be provided by GLM in the vicinity of a Global Precipitation Mission [*Smith et al.*, 2007] overpass would be much better suited for this

Table 3. Results of a Two-Sample Student's *t* Test Comparing the Optical Characteristics of LIS Flashes Between Land and Ocean[a]

		d.f.	μ_{land}	μ_{ocean}	*T* Score
Area (km^2)	day	8.4e5	205	266	154
	transition	7.2e5	248	318	138
	night	1.4e6	264	343	180
Radiance ratio	day	8.1e5	9.9	13.9	144
	transition	6.6e5	11.6	17.5	162
	night	1.3e6	11.7	18.1	211
Duration (s)	day	8.0e5	0.25	0.29	109
	transition	6.9e5	0.28	0.32	84
	night	1.3e6	0.29	0.32	72
Groups per flash	day	7.2e5	9.1	13.5	199
	transition	6.4e5	11.2	16.3	174
	night	1.3e6	12.0	16.7	190
Propagation factor	day	8.2e5	0.29	0.33	159
	transition	6.9e5	0.29	0.33	147
	night	1.4e6	0.29	0.33	125
Total radiance (J sr^{-1} µm^{-1})	day	7.1e5	12.5	23.8	146
	transition	6.0e5	12.6	24.3	164
	night	1.3e6	13.3	24.0	138
Mean optical power (W m^{-2} sr^{-1} µm^{-1})	day	9.2e5	0.62	0.75	30.6
	transition	5.7e5	0.37	0.49	33.6
	night	1.3e6	0.35	0.45	52.0

[a]Statistical significance at the $p < 0.001$ level requires *T* scores greater than 3.09.

type of analysis. In the meantime, a comparatively modest design was chosen that is based on four unique degrees of freedom: diurnal LIS sensitivity, ICF mean 85 GHz PCT, ICF mean PR storm height, and ICF maximum 20 dBZ height. This configuration allows for 31,000 unique species of ICFs that are more conductive to building up a robust sample for meaningful statistics.

A paired Student's *t* test is then performed by using this database to assess the differences in optical properties for land and ocean flashes that occur in otherwise similar clouds. Only similar cloud species that contain at least 100 samples are considered in this analysis. Complete distributions of the differences between land and ocean area and radiance ratio in similar clouds for each time of day are shown in Figure 9 with sample mean and

Table 4. Results of a Paired *t* Test Examining the Optical Characteristics of LIS Flashes That Illuminate Similar Clouds in Land and Ocean Regions

		N	μ_{land}	μ_{ocean}	*T* Score
Area (km^2)	day	975	191	255	42
	transition	1077	230	294	36
	night	1497	252	330	43
Radiance ratio	day	975	8.9	13.8	42
	transition	1077	10.7	16.8	36
	night	1497	10.8	17.9	43
Duration (s)	day	975	0.24	0.29	33
	transition	1077	0.26	0.31	30
	night	1497	0.24	0.30	39
Groups per flash	day	975	8.6	13.8	42
	transition	1077	10.2	15.8	42
	night	1497	10.5	16.1	50
Propagation factor	day	975	0.26	0.31	36
	transition	1077	0.26	0.31	33
	night	1497	0.22	0.28	42
Total radiance (J µm^{-1} sr^{-1})	day	975	16.4	33.1	37
	transition	1077	16.5	33.4	38
	night	1497	16.2	31.7	41
Mean optical power (W m^{-2} µm^{-1} sr^{-1})	day	975	0.70	0.78	12
	transition	1077	0.41	0.52	15
	night	1497	0.31	0.40	21

1-sigma values overlain. Not only are the mean differences between land and ocean positive for both parameters and at all times of day, but similar cloud species fall almost exclusively above zero. Oceanic flashes are brighter and larger in almost every scenario with all else being equal. The full results of the paired t test are presented in Table 4. For significance at the $p = 0.001$ level, T scores must exceed approximate 3 given the degrees of freedom in this analysis. Not only are the radiance ratio and area results in Figure 9 statistically significant, but oceanic flashes are also significantly longer-lasting, contain more groups, are more prone to propagation, and have higher total radiances and mean optical powers than those over land.

Of particular importance is the prevalence of oceanic flashes to propagate or contain a large number of groups. As they describe how an optical flash moves within the cloud as it evolves and the number of optical pulses it contains, respectively, they are indicative of variations in flash structure rather than energetics.

4. Conclusion

In this study, the optical properties of lightning flashes measured by the Lightning Imaging Sensor (LIS) are examined alongside PR, TMI, and VIRS properties of the cloud regions illuminated by each flash. A high degree of variability exists in optical flash characteristics that results from the energetics and structure of the flashes as well as radiative transfer within the cloud. These factors provide an important source of uncertainty for assessing trends in the optical lightning measurements, particularly for the future GLM and ISS-LIS platforms that will natively lack the suite of coincident measurements that were available on TRMM.

New optical lightning properties are discussed, including measures of horizontal flash propagation and elongation that take advantage of event pixel- and group-level LIS measurements. Propagation and elongation are both more common in oceanic lightning than in flashes onshore, with propagating flashes accounting for up to 30% of all lightning in subtropical ocean regions and elongated flashes accounting for up to 60% of all oceanic flashes in the inner tropics.

A database of illuminated clouds (ICFs) is used to assess whether the noted differences in optical flash properties between land and ocean are the result of flash energetics and structure or optical depth and associated radiative transfer effects. It is determined that even when LIS flashes illuminate similar cloud regions with comparable background radiances, statistically significant differences between their properties still exist. These results indicate that with all else being equal, oceanic flashes are typically more energetic and have different structures (i.e., more optical pulses per flash and more prone to horizontal propagation) than their land-based counterparts.

Acknowledgments
This work was partly funded by the National Science Foundation Frontiers in Earth System Dynamics grant 1135446 and the NSF grant 1519006. The National Center for Atmospheric Research is funded by the National Science Foundation. Data used in this study may be accessed via the data page at www.michaeljpeterson.net.

References

Bang, S. D., and E. J. Zipser (2015), Differences in size spectra of electrified storms over land and ocean, *Geophys. Res. Lett.*, *42*, 6944–6851, doi:10.1002/2015GRL065264.

Blakeslee, R. J., et al. (2014), *Lightning Imaging Sensor (LIS) for the International Space Station (ICC): Mission Description and Science Goals*, 1–15, XV Int. Conf. Atmos. Electricity, Norman, Okla.

Boccippio, D. J., S. J. Goodman, and S. Heckman (2000), Regional differences in tropical lightning distributions, *J. Appl. Meteorol.*, *39*, 2231–2248.

Burns, G. B., A. V. Frank-Kamenetsky, O. A. Troschichev, E. A. Bering, and B. D. Reddell (2005), Interannual consistency of bi-monthly differences in annual variations of the ground-level, vertical electric field, *J. Geophys. Res.*, *110*, D10106, doi:10.1029/2004JD005469.

Cecil, D. J. (2009), Passive microwave brightness temperatures as proxies for hailstorms, *J. Appl. Meteorol. Climatol.*, *48*, 1281–1286.

Cecil, D. J., S. J. Goodman, D. J. Boccippio, E. J. Zipser, and S. W. Nesbitt (2005), Three years of TRMM precipitation features. Part I: Radar, radiometric, and lightning characteristics, *Mon. Weather Rev.*, *133*, 543–566.

Cecil, D. J., D. E. Buechler, and R. J. Blakeslee (2014), Gridded lightning climatology from TRMM-LIS and OTD: Dataset description, *Atmos. Res.*, *1350–136*, 404–414.

Christian, H. J., R. J. Blakeslee, S. J. Goodman, and D. M. Mach (Eds) (2000), *Algorithm Theoretical Basis Document (ATBD) for the Lightning Imaging Sensor (LIS)*, NASA/Marshall Space Flight Center, Alabama. [Available at http://eospso.gsfc.nasa.gov/atbd/listables.html] posted 1 Feb. 2000.

Christian, H. J., et al. (2003), Global frequency and distribution of lightning as observed from space by the Optical Transient Detector, *J. Geophys. Res.*, *108*(D1), 4005, doi:10.1029/2002JD002347.

Coleman, L. M., M. Stolzenburg, T. C. Marshall, and M. Stanley (2008), Horizontal lightning propagation, preliminary breakdown, and electric potential in New Mexico thunderstorms, *J. Geophys. Res.*, *113*, D09208, doi:10.1029/2007JD009459.

Court, A., and J. F. Griffiths (1982), *Thunderstorm Climatology, Thunderstorms: A Social, Scientific, and Technological Documentary, Thunderstorm Morphology and Dynamics*, vol. 2, edited by E. Kessler, pp. 11–52 , U.S. Dep. of Commer., Washington, D. C.

Deierling, W., and W. A. Petersen (2008), Total lightning activity as an indicator of updraft characteristics, *J. Geophys. Res.*, *113*, D16210, doi:10.1029/2007JD009598.

Goodman, S. J., et al. (2013), The GOES-R geostationary lightning mapper (GLM), *J. Atmos. Res.*, *125–126*, 34–49.

Hays, P. B., and R. G. Roble (1979), A quasi-static model of global atmospheric electricity 1. The lower atmosphere, *J. Geophys. Res.*, *84*, 3291–3305, doi:10.1029/JA084iA07p03291.

Hutchins, M. L., R. H. Holzworth, K. S. Virts, J. M. Wallace, and S. Heckman (2013), Radiated VLF energy differences of land and oceanic lightning, *Geophys. Res. Lett.*, *40*, 2390–2394, doi:10.1002/grl.50406,2013.

Koshak, W. J. (2010), Optical characteristics of OTD flashes and the implications for flash-type discrimination, *J. Atmos. Oceanic Technol.*, *27*, 1822–1838.

Koshak, W. J., R. J. Solakiewicz, D. D. Phanord, and R. J. Blakeslee (1994), Diffusion model for lightning radiative transfer, *J. Geophys. Res.*, *99*, 14,361–14,371, doi:10.1029/94JD00022.

Koshak, W. K., M. F. Stewart, H. J. Christian, J. W. Bergstrom, J. M. Hall, and R. J. Solakiewicz (2000), Laboratory calibration of the Optical Transient Detector and the Lightning Imaging Sensor, *J. Atmos. Oceanic Technol.*, *17*, 905–915.

Kummerow, C., W. Barnes, T. Kozu, J. Shiue, and J. Simpson (1998), The Tropical Rainfall Measuring Mission (TRMM) sensor package, *J. Atmos. Oceanic Technol.*, *15*, 809–817.

Landsberg, H. (1960), *Physical Climatology*, 2nd ed., Gray Printing Co., Du-Bois, Pa.

Lay, E. H., A. R. Jacobson, R. H. Holzworth, C. J. Rodger, and R. L. Dowden (2007), Local time variation in land/ocean lightning flash density as measured by the World Wide Lightning Location Network, *J. Geophys. Res.*, *112*, D13111, doi:10.1029/2006JD007944.

Light, T. E., D. M. Suczcynsky, M. W. Kirkland, and A. R. Jacobson (2001), Simulations of lightning optical waveforms as seen through clouds by satellites, *J. Geophys. Res.*, *106*, 17,103–17,114, doi:10.1029/2001JD900051.

Liu, C., E. J. Zipser, D. J. Cecil, S. W. Nesbitt, and S. Sherwood (2008), A cloud and precipitation feature database from 9 years of TRMM observations, *J. Appl. Meteorol. Climatol.*, *47*, 2712–2728, doi:10.1175/2008JAMC1890.

Liu, C., E. R. Williams, E. J. Zipser, and G. Burns (2010), Diurnal variations of global thunderstorms and electrified shower clouds and their contribution to the global electric circuit, *J. Atmos. Sci.*, *67*, 309–323, doi:10.1175/2009JAS3248.1.

Lucas, G. M., A. J. G. Baumgaertner, and J. P. Thayer (2015), A global electric circuit model within a community climate model, *J. Geophys. Res. Atmos.*, *120*, 12,054–12,066, doi:10.1002/2015JD023562.

Mach, D. M., H. J. Christian, R. J. Blackeslee, D. J. Boccippio, S. J. Goodman, and W. L. Boeck (2007), Performance assessment of the Optical Transient Detector and Lightning Imaging Sensor, *J. Geophys. Res.*, *112*, D09210, doi:10.1029/2006JD007787.

Mach, D. M., R. J. Blakeslee, M. G. Bateman, and J. C. Bailey (2009), Electric fields, conductivity, and estimated currents from aircraft overflights of electrified clouds, *J. Geophys. Res.*, *114*, D10204, doi:10.1029/2008JD011495.

Mach, D. M., R. J. Blakeslee, M. G. Bateman, and J. C. Bailey (2010), Comparisons of total currents based on storm location, polarity, and flash rates derived from high-altitude aircraft overflights, *J. Geophys. Res.*, *115*, D03201, doi:10.1029/2009JD012240.

Mach, D. M., R. J. Blakeslee, and M. G. Bateman (2011), Global electric circuit implications of combined aircraft storm electric current measurements and satellite-based diurnal lightning statistics, *J. Geophys. Res.*, *116*, D05201, doi:10.1029/2010JD014462.

Orville, R. E., and R. W. Henderson (1986), Global distribution of midnight lightning: September 1977 to August 1978, *Mon. Weather Rev.*, *114*, 2640–2653.

Orville, R. E., and G. R. Huffines (2001), Cloud-to-ground lightning in the United States: NLDN results in the first decade, 1989–98, *Mon. Weather Rev.*, *129*, 1179–1193.

Peterson, M. J., and C. Liu (2011), Global statistics of lightning in anvil and stratiform regions over the tropics and subtropics observed by TRMM, *J. Geophys. Res.*, *116*, D23201, doi:10.1029/2011JD015908.

Peterson, M. J., and C. Liu (2013), Characteristics of lightning flashes with exceptional illuminated areas, durations, and optical powers and surrounding storm properties in the tropics and inner subtropics, *J. Geophys. Res. Atmos.*, *118*, 11,727–11,740, doi:10.1002/jgrd.50715.

Peterson, M. J., C. Liu, D. Mach, W. Deierling, and C. Kalb (2015), A method of estimating electric fields above electrified clouds from passive microwave observations, *J. Atmos. Oceanic Technol.*, *32*, 1429–1446.

Schultz, C. J., W. A. Peterson, and L. D. Carey (2009), Preliminary development and evaluation of lightning jump algorithms for real-time detection of severe weather, *J. Appl. Meteorol. Climatol.*, *48*, 2543–2563.

Smith, E. A., et al. (2007), International Global Precipitation Measurement (GPM) program and mission: An overview, in *Measuring Precipitation From Space*, pp. 611–653, Springer, Netherlands.

Spencer, R. W., H. G. Goodman, and R. E. Hood (1989), Precipitation retrieval over land and ocean with the SSM/I: Identification and characteristics of the scattering signal, *J. Atmos. Oceanic Tech.*, *6*, 254–273.

Takahashi, T. (1978), Riming electrification as a charge generation mechanism in thunderstorms, *J. Atmos. Sci.*, *35*, 1536–1548.

Thomason, L. W., and E. P. Krider (1982), The effects of clouds on the light produced by lightning, *J. Atmos. Sci.*, *39*, 2051–2065.

Vivekanandan, J., J. Turk, and V. N. Bringi (1991), Ice water path estimation and characterization using passive microwave radiometry, *J. Appl. Meteorol.*, *30*, 1407–1421.

Vonnegut, B. (1983), Deductions concerning accumulations of electrified particles in thunderclouds based on electric field changes associated with lightning, *J. Geophys. Res.*, *88*, 3911–3912, doi:10.1029/JC088iC06p03911.

Whipple, F. J. W. (1929), On the association of the diurnal variation of electric potential gradient in fine weather with the distribution of thunderstorms over the globe, *Q. J. R. Met. Soc.*, *55*, 1–17.

Williams, E. R. (2009), The global electrical circuit: A review, *Atmos. Res.*, *91*(2–4), 140–152, doi:10.1016/j.atmosres.2008.05.018.

Williams, E. R., T. Chan, and D. Boccippio (2004), Islands as miniature continents: Another look at the land-ocean lightning contrast, *J. Geophys. Res.*, *109*, D16206, doi:10.1029/2003JD003833.